Catalytic oxidation of glucose over highly stable Au_xPd_y NPs immobilised on ceria nanorods

Motaz Khawaji[a,1], Inês Graça[a,2] , Ecaterina Ware[b], David Chadwick[a,*]

[a] Department of Chemical Engineering, Imperial College London, London, SW7 2AZ, UK
[b] Department of Materials, Royal School of Mines, Imperial College London, London, SW7 2AZ, UK

*Corresponding author: d.chadwick@imperial.ac.uk

Abstract

The catalytic performance of Au_xPd_y nanoparticles prepared by colloidal synthesis and immobilised on ceria nanorods (Ce-NR) in the selective oxidation of glucose has been studied under initially basic and relatively mild conditions. Activity was found to be strongly dependent on the bimetallic composition with Au-rich catalysts being more active in glucose oxidation. Catalyst recycling revealed negligible deactivation or metal loss from leaching, and continuing high selectivity to gluconic acid (≥97.7%). Defects on the Ce-NR surface appear to serve as anchoring sites for Au-Pd NPs giving rise to small and very stable NPs.

Keywords: glucose; gold-palladium; ceria; oxidation; gluconic acid

[1] Present address: Chemicals R&D at KAUST, Saudi Aramco R&D Center, Thuwal 23955, Saudi Arabia.
[2] Present address: University of Aberdeen, School of Engineering, King's College, Aberdeen, AB24 3UE, UK.

1 Introduction

Valorisation of bio-renewable resources by conversion to chemical products is currently the subject of intensive research. In particular, sugars derived from biomass can provide a versatile platform for the production of high-value chemicals [1] in which the selective oxidation of glucose to gluconic acid, and its further oxidation to glucaric acid are important steps. Gluconic acid (GLO) and its salts have a large number of applications in several industries such as the food and pharmaceuticals industries [2-4]. Glucaric acid (GLA) has been classified by the U.S. Department of Energy as one of the "top value-added chemicals" derived from biomass [5] and is considered to be a potential bio-derived intermediate in the synthesis of adipic acid [5-7]. Currently, GLO and its salts are produced mainly via the enzymatic oxidation of glucose [2], while GLA is produced primarily by glucose oxidation with nitric acid [8, 9]. The use of heterogeneous catalysts for the direct catalytic selective oxidation of glucose under mild conditions is an attractive alternative to current processes, and could lead to a lower environmental impact [10, 11].

The oxidation of glucose to gluconic acid (or it salts) with air, O_2 or H_2O_2 over heterogeneous catalysts has been studied extensively, mainly over Pd or Pt supported on carbon [12-14]. It has been shown that Au and Au alloys are also good catalysts for the oxidation of glucose to gluconic acid [15-17]. The activity and selectivity of Au nanoparticles (NPs) have been ascribed to the ability of gold to resist oxygen poisoning and to convert the aldose groups to their corresponding aldonic acids such as gluconic acid [18, 19]. Under mild reaction conditions, the optimal pH for the selective oxidation of glucose to GLO with transition metal catalysts is typically 9-11. In this pH range, metal leaching and catalyst deactivation are significantly reduced, and lactone formation is minimised [20]. A gluconic acid selectivity above 98% can be attained at these conditions [3]. Interest in the production of GLA from glucose has increased significantly since it has been recognised as an important platform [5] and GLA yields over 70% have been reported in both acidic and basic conditions using Pt based catalysts [21, 22]

The separation of gluconate and glucarate salts, which are the products under basic conditions, is easier than the separation of the free acids. Armstrong *et al.* [21] have recently reported on a new process based on ion exchange and azeotropic evaporation for the recovery of high purity glucaric acid (> 99.96%) from the glucarate salts. This approach avoids formation of lactone and dilactone glucarate derivatives, which can arise easily during separation and water removal. In principle, therefore, the use of base in the catalytic oxidation of glucose can be justified by catalytic performance and ease of product separation. Catalysts containing gold are often not the most promising in acidic conditions due to significant leaching. The use of high pH makes Au-based catalysts more attractive for glucose selective oxidation.

We have recently reported on the catalytic activity of bimetallic Au-Pd NPs prepared by colloidal synthesis and immobilised on titanate nanotubes (Ti-NT) for the selective oxidation of

glucose [22]. Ti-NTs have large surface area and high surface hydroxyl group density (ca. 5.8 OH/nm^2) [23]. These physiochemical and morphological properties make Ti-NT very attractive as a catalyst support. The Au-Pd NPs are located on the external surfaces of Ti-NT as opposed to the internal pore volume or interstitial sites of Ti-NT, allowing easy accessibility of the reactants to the active metal sites, and product escape [24]. In addition to being active catalysts for glucose oxidation, it was shown that the yield of GLA is close to linearly dependent on the atomic composition of Au in the Au-Pd catalysts [22]. However, it was speculated that this apparent correlation of GLA yield with Au content was associated with catalytically active Au nanoclusters in solution produced by leaching of Au, as demonstrated in a recent study of hydrocarbon oxidation on Au catalysts [25]. Ceria is also well known as a good support for Au and Pd NPs as catalysts for oxidation [26-30]. We have shown recently that in fact Au-Pd supported on nanostructured ceria supports, particularly ceria nanorods, are superior to Ti-NT in the solvent-less selective oxidation of benzyl alcohol over Au-Pd [31]. This superiority of ceria based catalysts over Ti-NT was attributed to a combination of several factors: the metal-support interaction and the high Au-Pd surface concentration, which is related to the ability of the Ce-NR surface to stabilise highly-dispersed Au-Pd NPs, and the high concentration of oxygen vacancies in Ce-NR surface which can activate oxygen [31-33]. It follows that Au-Pd/Ce-NR are likely to be good catalysts for the oxidation of glucose.

In this paper we report for the first time the catalytic performance of Au, Pd, and Au_xPd_y NPs immobilised on CeO_2 nanorods in the selective oxidation of glucose under relatively mild and basic conditions with molecular oxygen. Ceria nanorods (Ce-NR) have been used as support since as noted above Au-Pd supported on ceria nanorods have been shown previously to be highly active catalysts for selective oxidation [31, 34, 35]. Of particular interest are the catalytic activity and selectivity to gluconic and glucaric acids, and the dependence on NP bimetallic composition. The high dispersion and high degree of alloying of Au-Pd NPs prepared by colloidal synthesis and immobilised on the nanostructured ceria support make these ideal materials to examine the dependence of activity and selectivity on bimetallic alloy composition. It is shown for glucose oxidation that under initially basic conditions, the addition of Au atoms to Pd NPs leads to enhancement in the catalytic activity reaching a maximum at 61 at.% Au in the Au-Pd NP, while the selectivity to gluconic acid remains essentially independent of composition at > 98%. This is in sharp contrast to the behaviour over Au-Pd/Ti-NT reported previously [22]. A study of recycling of a representative Au-Pd/Ce-NR catalyst in glucose oxidation showed the catalyst to be exceptionally stable in terms of both activity and selectivity.

2 Materials and methods

2.1 Materials

All chemical reagents and metal precursors and were purchased from Sigma Aldrich and used as received: NaOH (99.99% trace metals basis), H_2SO_4(≥97.5% purity), $Ce(NO_3)_3{\cdot}6H_2O$, poly(vinyl alcohol) (PVA) (MW 9,000-10,000, 80% hydrolyzed), $HAuCl_4.3H_2O$ (99.999% purity), $PdCl_2$ (5 wt.

% in 10 wt. % HCl), $NaBH_4$ (Aldrich ≥98.0%), D-glucose (>99.5% purity), gluconic acid (49-53 wt. % in H_2O), glycolic acid (99% purity), oxalic acid (≥99.0% purity), fructose (≥ 99% purity). Glucaric acid with 99.96% purity was provided by Cardiff Catalysis Institute. O_2 (100% pure) for catalytic tests was supplied by BOC.

2.2 Catalyst preparation

Synthesis of ceria nanostructures

Ceria nanorods were prepared by the alkaline hydrothermal treatment method reported previously [36]. Usually, 0.6 g of $Ce(NO_3)_3.6H_2O$ was added to a 40 mL of NaOH solution of 15M and stirred for 1h in a 45 mL PTFE-lined autoclave. The autoclave was then placed in an air-circulating oven for 24 hours at 100°C. Following the hydrothermal synthesis, the autoclave was cooled down to room temperature and the powder obtained was filtered, washed several times with both deionized water and a deionized water-ethanol mixture, and dried overnight at 120°C. The dried powder was calcined at 400°C for 4h in synthetic air with a flow rate of 100 mL/min, and a heating rate of 10°C/min.

Catalyst preparation by sol-immobilisation

The Au-Pd colloidal solution was prepared following previously reported procedures [22, 35]. The Ce-NR supports were acidified to a pH value of 3.0 (i.e. below the PZC of Ce-NR) by the drop-wise addition of 1.0 M solution of H_2SO_4. The zeta potential of Ce-NR has been studied previously and the PZC of Ce-NR was reported to be ca. 8.5 [31]. The Au-Pd colloidal NPs were produced by dissolving $HAuCl_4.3H_2O$ and $PdCl_2$ in 100 mL of de-ionised (DI) water at 5°C while stirring vigorously. Subsequently, 2,400 mg of 1.0 wt.% PVA solution was freshly prepared at room temperature and added to the metal precursors solution and stirred. The weight ratio of PVA/(Au+Pd) was maintained at 1.2. The amount of metal precursors dissolved in DI water was as follows: Au/Ce-NR ($HAuCl_4{\cdot}3H_2O$ = 0.102 mmol), Pd/Ce-NR ($PdCl_2$ = 0.189 mmol), $Au_{61}Pd_{39}$/Ce-NR ($HAuCl_4{\cdot}3H_2O$ = 0.153, $PdCl_2$ = 0.047mmol), $Au_{39}Pd_{61}$/Ce-NR ($HAuCl_4{\cdot}3H_2O$ =0.051, $PdCl_2$= 0.094 mmol), $Au_{21}Pd_{79}$/Ce-NR ($HAuCl_4{\cdot}3H_2O$ = 0.026 mmol, $PdCl_2$ = 0.142 mmol). The metal precursors were reduced by the addition of 7.5 mL of 0.1 M $NaBH_4$ ($NaBH_4$:(Au+Pd)=5:1 molar ratio). The Au-Pd colloid was left stirring at 1,500 rpm for 1h before 1.0 g of the acidified support was added. The slurry was stirred for 1h, filtered, and washed with DI water several times until the pH of the mother liquor reached ~7.0.

The catalysts were dried overnight at 100 °C, and refluxed in hot water (90°C) for 60 minutes, filtered and dried again overnight at 100 °C. The dried catalysts were used without any further treatment. All the monometallic and bimetallic catalysts prepared in this study had nominal metal loadings of 2.0 wt.%.

2.3 Reaction procedure

Glucose oxidation was carried out in a 25 mL glass-lined miniclave (Buchiglas, Switzerland) reactor. In a typical run, glucose solution (3.0 mL, 0.25 M, $pH_{initial}$ = 9.5) and the prerequisite amount of catalyst (ca. 50-90 mg) were added to the reactor. The glucose: catalytic metal molar ratio was 100:1, and Na:glucose = 1:7900 mol/mol. The pH of the reaction solution was adjusted by addition of NaOH. The reactor was purged three times with pure O_2 before being pressurised to the desired pressure (6 bar at room temperature). The temperature of the reactor was subsequently set to 80˚C, and reactor was stirred at 1000 rpm. At the end of each reaction, the reactor was cooled down to ambient temperature and vented slowly. Subsequently, 7.0 mL DI water was added to the reactor to dilute the reaction mixture. The catalyst was separated from the liquid phase by centrifugation at 5000 rpm for 20 minutes. A sample (7.0 mL) was taken from the supernatant and mixed with 50 μL formic acid (internal standard) for product analysis. Analysis of the reaction products was carried out using HPLC (CTO-20AC, Shimazdu, Japan) fitted with a SUPELCOGEL$_{TM}$ C-610H HPLC column (30 cm x 7.8 mm ID, filter: 25 mm ID with 0.45 μm pores) and UV and refractive index detectors, using 0.1 % v/v phosphoric acid as the mobile phase. HPLC was calibrated with high purity standards acquired from Sigma Aldrich prior to product analysis. The spent catalyst was collected at the end of each run and washed several times with diluted ethanol (20 vol.% in water), and centrifuged before it was dried overnight at 90 ˚C. The dried catalyst was then used in the following reaction cycle. The conversion of glucose (X_G), product yield (Y_i), selectivity (S_i), and carbon balance were calculated using the following equations:

$$X_G\ (\%) = \frac{n_{initial\ glucose} - n_{final\ glucose}}{n_{initial\ glucose}} \times 100$$

$$Y_i\ (mol\%) = \frac{n_{product\ i}}{n_{initial\ glucose}} \times 100$$

$$S_i (mol\%) = \frac{n_{product\ i}}{\Sigma\, n_{product\ i}} \times 100$$

$$Carbon\ balance\ (\%) = \frac{initial\ moles\ of\ carbon}{final\ moles\ of\ carbon} \times 100$$

Where *n* is the number of moles of glucose or carbon containing product *i*. The standard deviation in the carbon balance was 2.8%.

2.4 Catalyst characterisation

X-ray diffraction (XRD) measurements were recorded using a PANalytical X'Pert Pro Multi-Purpose Diffractometer using CuKα radiation. The analysis was conducted over a scan angle of 2θ=5–70° with a step size 0.0167°. The bulk metal loading was determined using ICP-OES by

MEDAC Ltd. (UK). TEM images were obtained using a JEOL JEM-2100F microscope operating at 200 kV. Typically, samples were dispersed in ethanol and sonicated for 30 min before being dispersed on copper grids with a lacy carbon film (300 mesh size). The particle size distribution and average particle size of the metal NPs were determined from the TEM images by analysing 100 randomly selected NPs. X-ray photoelectron spectroscopy (XPS) measurements were acquired using a Thermo K-Alpha Spectrometer equipped with an Al Kα source gun. Samples were fixed on adhesive carbon tape, and the spectra were collected using an X-ray spot size of 400 μm with a pass energy of 20 eV and 0.1 eV increments. The binding energies (B.E.) were referenced to the C 1s peak of adventitious carbon at 284.8 eV. The error in the XPS measurement is typically ± 0.2 eV. XPS data were analysed using Avantage software provided by Thermo Scientific.

3 Results and discussion

3.1 Characterisation of ceria nanostructures

Characterisation of the as-synthesised Ce-NR by TEM, XRD, and nitrogen adsorption-desorption measurements has been reported previously [35]. The BET surface area of the Ce-NR support was 61.7 m^2/g. The rod-like shape of Ce-NR is clearly visible in the TEM images (Figure S1a). The XRD patterns for the ceria nanorods are shown in Figure S1b. Cerium oxides display a crystalline structure with multiple sharp diffraction peaks at 2θ of 28.5°, 33.0°, 47.4°, 56.3°, and 69.6°, which respectively correspond to the (111), (200), (220), (311), (400) crystalline planes of the pure cubic phase (ceria fluorite structure, JCPDS 34-0394) [37].

In the Ce 3d XPS spectra of Ce-NR (Figure S2), two primary peaks associated with Ce^{4+} appear at ~882.5 and 901.1 eV and correspond to Ce $3d_{5/2}$ and Ce $3d_{3/2}$, respectively; while four additional satellite peaks assigned to Ce^{4+} appear at ~889.1, 989.8, 907.6, and ~916.9 eV. The peaks at ~880.5, 885.6, 898.5, and 903.1 eV are assigned to Ce^{3+}[37-39]. Deconvolution of the 3d XPS spectra showed a high concentration of Ce^{3+} (ca. 31%) for the as-synthesized ceria nanorods.

3.2 Catalyst characterisation

All the catalysts were prepared by sol-immobilisation using the procedure described in 2.2 above. The adsorption of colloidal metal NPs is strongly influenced by the surface charge of the support and the metal NPs. It is vital, therefore, that the surface charge of the support is determined beforehand, and the pH is controlled to enhance the adsorption of the metal sol. The zeta potentials of the Ce-NR support and Au-Pd sol as a function of pH and the PZC were determined previously [35]. The actual final metal compositions for the various catalysts used in this study are given in Table 1. The actual metal loadings of the catalysts were found to be reasonably close to the nominal loadings.

Table 1 Catalyst bulk composition.

Catalyst	Au (wt.%)	Pd (wt.%)	actual weight

	nominal	actual [a]	nominal	actual [a]	ratio Pd/Au
Au/Ce-NR	2.00	1.70	-	-	-
Pd/Ce-NR	-	-	2.00	1.72	-
$Au_{61}Pd_{39}$/Ce-NR	1.50	1.47	0.50	0.50	0.34
$Au_{39}Pd_{61}$/Ce-NR	1.00	1.13	1.00	0.94	0.83
$Au_{21}Pd_{79}$/Ce-NR	0.50	0.49	1.50	1.00	2.04

[a] Bulk composition; weight percentage per gram of sample, obtained by ICP-OES analysis.

The XRD diffraction patterns of the various monometallic and bimetallic Ce-NR supported catalysts are shown in Figure 1. The monometallic gold catalyst (i.e. Au/Ce-NR) displayed a weak and rather broad peak at 38.41°, which is ascribed to the pure Au(111) reflection plane. The bimetallic catalyst rich in gold (i.e. $Au_{61}Pd_{39}$/Ce-NR) displayed an Au(111) peak at a higher 2θ as a result of the change in the lattice constant and the formation of a Pd-Au alloy phase [40]. No clear diffraction peaks corresponding to either Au or Pd were detected in Pd/Ce-NR or the other Pd-rich bimetallic catalysts due to the low metal concentration and relatively small metal particle size (<4 nm).

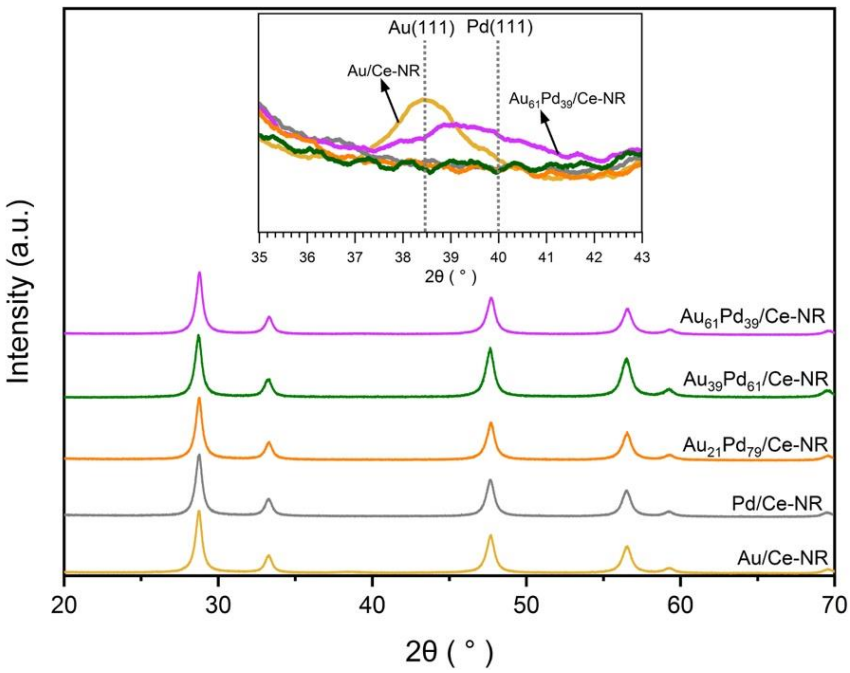

Figure 1 XRD of Au-Pd/Ce-NR catalysts. Au(111) reflection planes are shown in the inset.

HRTEM and STEM images of the various catalysts are shown in Figures 2. The bimetallic catalysts exhibited similar particle size distributions and mean particle sizes (2.1 to 2.9 nm), indicating that the bimetallic composition does not strongly influence the final particle size distribution on the Ce-NR support. The metal dispersion in Table 2 was calculated from the particle size distribution determined from TEM using the approximation method reported by Mori et al. [41]. The Au-Pd/Ce-NR catalysts showed a shallow maximum in dispersion (ca. 55%) at an intermediate Au content of 39 at.% (i.e. $Au_{39}Pd_{61}$/Ce-NR).

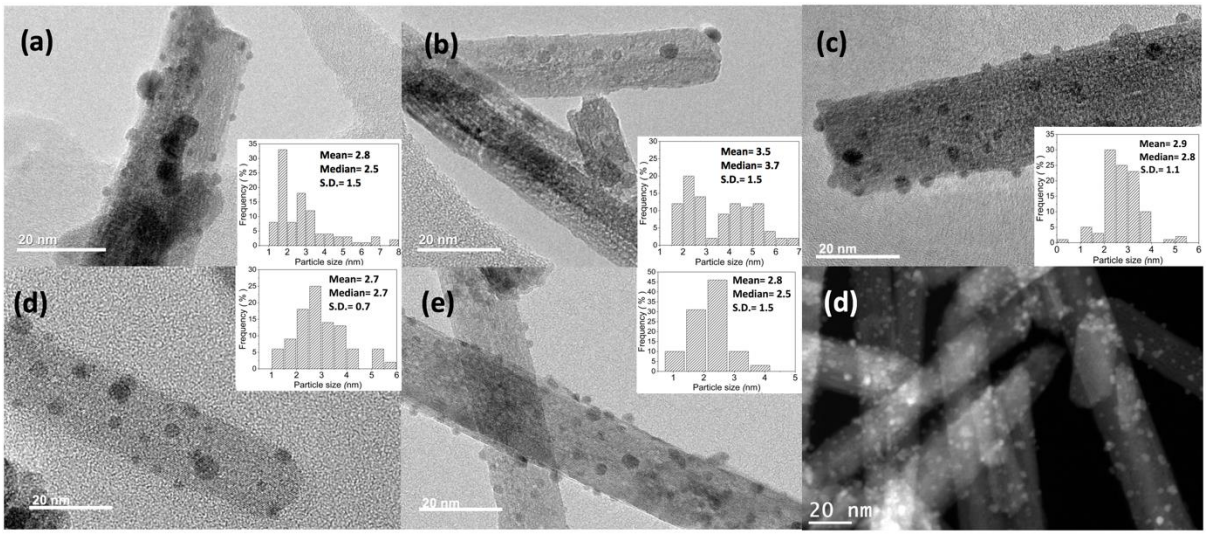

Figure 2 HRTEM image of (a) Au/Ce-NR, (d) Pd/Ce-NR, (c) $Au_{61}Pd_{39}$/Ce-NR, (d) $Au_{39}Pd_{61}$/Ce-NR, and (e) $Au_{21}Pd_{79}$/Ce-NR. The inset in each figure represents the corresponding particle size distribution. (d) STEM image of $Au_{21}Pd_{79}$/Ce-NR.

Table 2 Physicochemical properties of catalysts.

Catalyst	**Mean particle size (nm)** [a]	Metal dispersion (%) [a, b]
Au/Ce-NR	2.8 ± 1.5	47
Pd/Ce-NR	3.5 ± 1.5	32
$Au_{61}Pd_{39}$/Ce-NR	2.9 ± 1.1	44
$Au_{39}Pd_{61}$/Ce-NR	2.1 ± 0.7	55
$Au_{21}Pd_{79}$/Ce-NR	2.7 ± 0.7	46

[a] Determined from the particle size distribution from TEM
[b] See ESI for calculation details

The XPS spectra for Au 4f and Pd 3d are shown in Figures 3 and 4, respectively. The binding energy (B.E.) of the Au $4f_{7/2}$ component for the monometallic gold catalyst (Au/Ce-NR) was observed at 83.8 eV, while the bimetallic catalysts (Au_xPd_y/Ce-NR) exhibited Au $4f_{7/2}$ peaks at lower binding energies. The doublet peak appearing at >87 eV arises from the Au $4f_{5/2}$ component. The negative peak shift in the B.E. (Figure 3) is indicative of the close interaction between the Au and Pd atoms and the formation of an Au-Pd alloy phase[42].

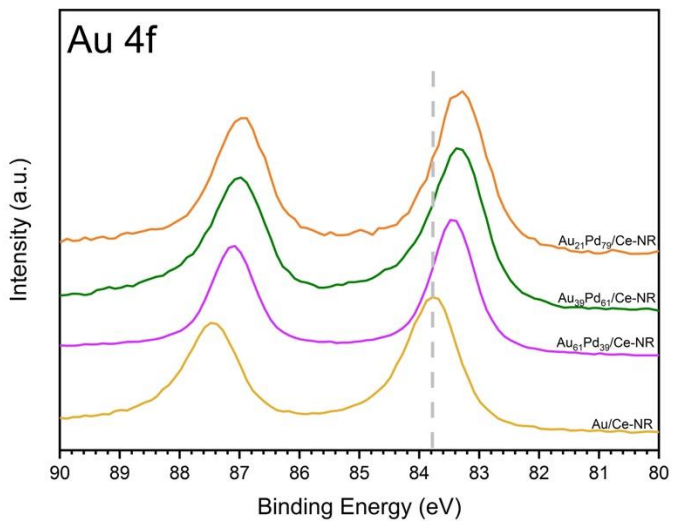

Figure 3 XPS of Au-Pd/Ce-NR catalysts.

The Pd 3d spectra for Pd/Ce-NR and Au_xPd_y/Ce-NR catalysts imply the presence of both metallic palladium (Pd^0) and oxidized palladium species (i.e. $Pd^{\delta+}$) in the dried catalysts. The Pd 3d spectra were deconvoluted using one component for Pd^0 and two components for Pd^{2+} and Pd^{4+} (Figure 4). The portion of metallic and oxidised palladium species present in each catalyst was determined from the fitted Pd 3d spectra and are given in Table 3. The XPS analysis revealed the presence of a high concentration of oxidised palladium species (ca. 76%) on the surface of catalyst Pd/Ce-NR. Although the presence of $Pd^{\delta+}$ species is expected due to surface oxidation arising from drying and storage of the catalysts as was also observed previously for Pd/Ti-NT [22], the markedly high concentration of oxidised Pd species suggest that it is likely to be related to the ability of the ceria support to supply oxygen to the metal NPs (i.e. via oxygen spillover).

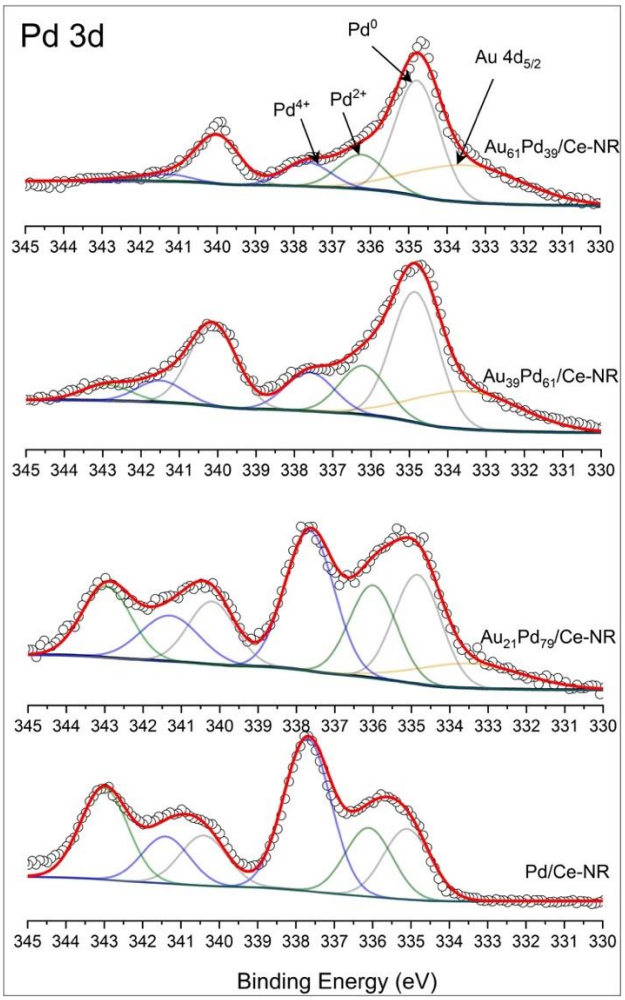

Figure 4 XPS spectra of Pd 3d for Pd/Ce-NR and Au_xPd_y/Ce-NR catalysts.

As the Au content increases (i.e. ratio Au/Pd increases) the proportion of Pd^0 increases with respect to $Pd^{\delta+}$, so that the catalyst with the highest gold content (i.e. $Au_{61}Pd_{39}$/Ce-NR) displayed the lowest concentration of $Pd^{\delta+}$ (see Table 3). These results are in agreement with earlier findings for Au-Pd/Ti-NT catalysts in relation to the impact of Au content on $Pd^{\delta+}$ concentration [22]. However, catalysts supported on Ce-NR exhibit consistently higher $Pd^{\delta+}$ concentration than similar bimetallic compositions supported on Ti-NT. This observation underlines the fact that ceria is able to supply surface oxygen to the metal NPs.

Table 3 Quantitative XPS data for the different catalysts

Catalyst	Binding Energy (eV)		(Au + Pd)/Ce [a]	Pd 3d	
	Au^0	Pd^0		Pd^0 (%)	$Pd^{\delta+}$ (%) [b]
Au/Ce-NR	83.8	-	0.07	-	-
Pd/Ce-NR	-	335.1	0.15	24	76
$Au_{61}Pd_{39}$/Ce-NR	83.5	334.8	0.15	66	34
$Au_{39}Pd_{61}$/Ce-NR	83.4	334.9	0.21	59	41
$Au_{21}Pd_{79}$/Ce-NR	83.3	334.9	0.12	32	68

[a] Atomic ratio from Au 4f, Pd 3d and Ce 3d.

[b] Combined value for Pd^{2+} and Pd^{4+} species.

The surface atomic composition of the catalysts was estimated from the fitted XPS data. The atomic ratio of Au/Pd, and (Au+Pd)/Ce for the different catalysts is given in Table 3. The high Au+Pd/Ce ratio in both the monometallic and bimetallic catalysts implies high metal surface concentration and highlights the advantage of using sol-immobilisation and Ce-NR as a catalyst support. For low loadings on the same support, the XPS surface ratios (Au+Pd)/Ce give a reasonably accurate assessment of the variations in metal dispersion of the various catalysts and are consistent with the variation in values from TEM.

3.3 Catalytic reaction

The selective oxidation of glucose was run under initially basic conditions with no adjustment of the pH during the runs as done in the earlier study of Au_xPd_y/Ti-NT and at the same reaction conditions: T=80°C, pH=9.5, and pO_2=6.0 [22]. Typically, 50-90 mg of catalyst was loaded into the reactor. In this range of catalyst weight, the reactions are kinetically controlled with no evidence of mass transfer limitations.

3.3.1 Composition dependence of selective oxidation of glucose

The two major products in the selective catalytic oxidation of glucose were gluconic acid (GLO) and glucaric acid (GLA). Several other minor side products such as oxalic acid, 5-ketogluconic acid, and glycolic acid can also be produced during glucose oxidation. Furthermore, isomerisation products such as fructose and mannose can also be produced in the process. Nonetheless, these by-products were minimal in the present study, and the Ce-NR supported catalysts exhibited very high selectivity to the primary selective oxidation product, GLO.

Glucose conversion and product selectivity for the various ceria-supported catalysts are given in Table 4. In the absence of any catalyst, a glucose conversion of ca. 5.8% was obtained as a result of glucose isomerisation to fructose under the mildly basic reaction conditions used. In the presence of catalyst, negligible isomerisation was detected. Regardless of the bimetallic composition, the different Au_xPd_y/Ce-NR catalysts displayed fairly similar selectivity to the primary oxidation product gluconic acid (GLO) of over 97%. This is quite different to the behavior of glucose oxidation over Au and Au-Pd/Ti-NT (see Table 5) catalysts where selectivity to glucaric acid reached 18-19% at the same 6h reaction-time under the same conditions [22]. The mean particle size of the Ce-NR supported NPs (ca. 2-3nm) is smaller than for Ti-NT (ca. 4-5nm) suggesting that the NP-support interaction is stronger in the case of ceria [35]. The impact of this on the selectivity and stability is discussed further below.

Table 4 Catalytic performance of the catalysts in the selective oxidation of glucose.

Catalyst	Conversion [a] (%)	Product selectivity (%) [b,c]						Carbon balance (%)
		GLO	GLA	GY	OX	TA	FT	
No catalyst	5.8	nd [c]	nd [c]	nd [c]	nd [c]	nd [c]	100	97
Au/Ce-NR	46.7	98.8	0.7	0.3	nd [c]	0.2	nd [c]	94
Pd/Ce-NR	4.7	99.6	0.4	0.0	nd [c]	nd [c]	nd [c]	101
$Au_{61}Pd_{39}$/Ce-NR	100	97.7	1.7	0.2	0.1	0.3	nd [c]	99
$Au_{39}Pd_{61}$/Ce-NR	64.4	97.9	1.9	0.1	0.1	nd [c]	nd [c]	101
$Au_{21}Pd_{79}$/Ce-NR	37.4	99.2	0.8	nd [c]	nd [c]	nd [c]	nd [c]	96

[a] Reaction conditions: T= 80°C, pO_2 =6 bar, stirring rate=1000 rpm, glucose conc. = 0.25 M, $pH_{initial}$= 9.5, glucose/metal (mol/mol)= 100, time=6h.
[b] Product selectivity: GLO = gluconic acid; GLA = glucaric acid; FT = Fructose. GY = glycolic acid; OX = oxalic acid; TA= tartronic acid were detected only in very low levels.
[b] nd = not detected.

The dependence of glucose conversion on the Au-Pd composition in the catalyst series Au_xPd_y/Ce-NR is shown in Figure 5. Pd/Ce-NR was found to have a very low activity for glucose oxidation, while Au/Ce-NR displayed moderate activity. For glucose oxidation, Au is catalytically more active than Pd in alkaline medium due to the promoting role of OH^-. It is also known that Pd is very prone to deactivation by oxygen poisoning during glucose oxidation. This is one of the reasons that Pd is often modified with promoters to improve its resistance to deactivation by oxygen poisoning [43]. Activity as measured by glucose conversion rises steadily with increasing Au content reaching a maximum at 61 at.% Au (the maximum Au content in Au-Pd studied) after which it declines and reaches a lower value at 100% Au. The bimetallic catalysts were considerably more active than the closest monometallic catalyst in terms of composition, highlighting the synergetic effect between Au and Pd. It has been suggested in the literature that negatively charged Au surface atoms are the active sites in glucose oxidation, and that the concentration of these negatively charged Au atoms is higher in very small Au clusters and in the presence of alloying elements such as Pd [44]. This is reflected in the negative chemical shift in Au 4f discussed above.

The composition dependence of activity for glucose oxidation exhibited by Au_xPd_y/Ce-NR in Figure 5 is quite different to that exhibited by Au_xPd_y/Ti-NT catalysts, where although the conversion was also higher for Au_xPd_y than for Pd/Ti-NT, it was effectively independent of Au content in the NPs at the same reaction conditions as used in the present study [22]. In addition, the most active Au_xPd_y/Ce-NR supported catalyst studied here, is notably more active than any Au_xPd_y/Ti-NT catalyst (100% conversion for $Au_{61}Pd_{39}$/Ce-NR versus 57-73% for Au_xPd_y/Ti-NT).

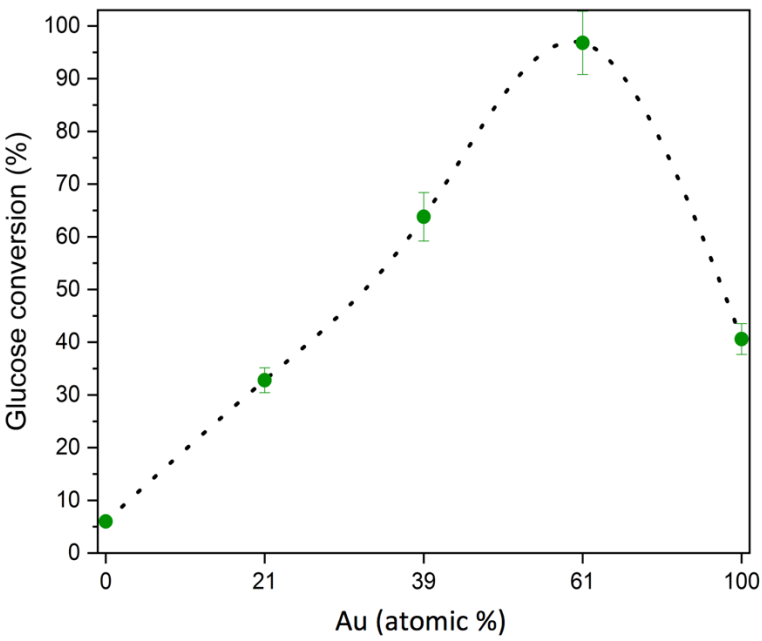

Figure 5. Glucose conversion as a function of Au content in Au_xPd_y for Ce-NR supported catalysts. Reaction conditions: T= 80°C, pO_2 =6 bar, stirring rate=1000 rpm, glucose= 0.25M, $pH_{initial}$ = 9.5, glucose/metal = 100, time=6h. Error bars represent the standard deviation in conversion.

The higher activity of Ce-NR supported catalysts compared to Ti-NT supported catalysts is likely to be associated with several factors. Firstly, the Au-Pd metal dispersion on the Ce-NR is higher than Au-Pd NP dispersion on Ti-NT, which we assume reflects a stronger metal NP-support interaction. Secondly, the redox properties and local basicity of the ceria surface itself. Recent studies have shown that both the redox properties and acid-base properties of ceria nanostructures are shape-dependent [45]. Ceria nanorods often expose a mixture of (110) and (100) surfaces, and the different exposed facets results in a highly defective surface [36]. These defect sites have been shown to play an important role in the stabilization of small metal NPs, which tend to form preferentially on the surface defects sites where the contact area with the support is maximized [46]. The result is a stronger metal support interaction and small NPs in the case of the present Au-Pd catalysts. In addition, the surface oxygen vacancies of Ce-NR contribute to the surface basicity and are able to activate oxygen thereby increasing the activity for selective oxidation catalysis [45].

Rather surprisingly, the present Au/Ce-NR catalyst is less active than the Au/Ti-NT catalyst [22]. Furthermore, the Ce-NR supported catalysts are highly selective for gluconic acid and show almost no activity for the deep oxidation to glucaric acid at the conditions used, in contrast to Au-Pd supported on Ti-NT [22]. Previously, we speculated that the oxidation of gluconic to glucaric acid might be catalyzed by Au nanoclusters leaching into solution, following the recent study of cyclooctene epoxidation by Qian et al [25], and that this explained the apparent strong correlation of glucaric acid yield with Au content. The Au and Au-Pd particle sizes on Ti-NT are in the range 3-5nm, while on the Ce-NR support the NPs are less than 3nm. We speculate that the smaller NP size on the Ce-NR support and the stronger metal-support interaction leads to a suppression of the release of

Au nanoclusters. Conversely, the larger Au and Au-Pd NPs on the Ti-NT support probably reflects a weaker metal-support interaction, which releases Au nanoclusters more easily. Indeed, we show below that the Ce-NR supported catalysts are very stable with negligible leaching, in contrast to Au and Au-Pd supported on Ti-NT [22]. As a consequence, oxidation to glucaric acid hardly takes place on the Ce-NR supported catalysts.

The differing dependence of activity on Au_xPd_y composition for Ce-NR and Ti-NT supported catalysts may also be related to their respective stabilities. Possibly, the exposed surfaces of the Au-Pd NPs on Ti-NT are Au-rich due to the leaching, whereas on the more stable Ce-NR supported NPs the surface composition is closer to the bulk values.

The activities of the present catalysts are compared in Table 5 with recent studies of glucose oxidation in the literature. The Au-Pd/Ce-NR catalyst has comparable activity to Pt catalysts. Although $PtCu_3/TiO_2$ has superior GLO productivity, which to an extent reflects the very high basic conditions used (pH>13), it is notably less selective.

Table 5 Comparison of the catalytic performance of monometallic and bimetallic catalysts

Catalyst	pH	T (°C)	P (bar)	Time (h)	Conversion (%)	Selectivity (mol%)		Productivity GLO	Ref.
						GLO	GLA	mol mol^{-1} h^{-1}	
Au/Ce-NR	9.5 uncontrolled	80	6.0 O_2	6	46.7	98.8	0.7	7.7	This study
$Au_{61}Pd_{39}$/Ce-NR	9.5 uncontrolled	80	6.0 O_2	6	100.0	97.7	1.7	16.3	This study
Au/Ti-NT [b]	9.5 uncontrolled	80	6.0 O_2	6	73	75.6	18.5	9.2	[22]
$Au_{15}Pd_{85}$/Ti-NT [b]	9.5 uncontrolled	80	6.0 O_2	6	64	98.1	1.7	10.5	[22]
Au/TiO_2 [b]	9.5 uncontrolled	80	6.0 O_2	6	9.3	99.9	0.1	1.5	[22]
Pt/C [c]	9.5 uncontrolled	80	6.0 O_2	10	97	83	16.0	8.1	[22]
Pt/SiO_2 [c]	9.5 uncontrolled	80	6.0 O_2	10	45	93	7.0	4.2	[22]
Au/C	9.5 controlled	50	1.0 air	0.5	100	>99	-	-	[15]
Pt/C	8.5 uncontrolled	80	6.2 O_2	1	100	41	58	22.1[a]	[47]
Pt_1Cu_3/TiO_2	pH>13 uncontrolled	45	1.0 O_2	6	100	38	9	65.0[a]	[48]

[a] Values calculated based on data provided in literature.
[b] Catalyst prepared by sol-immobilisation.
[c] Catalyst obtained from a commercial vendor.

3.3.2 Catalyst recycling in glucose oxidation

The catalytic performance of the most active Ce-NR supported catalyst ($Au_{61}Pd_{39}$/Ce-NR) was assessed with repeated usage, since catalyst stability and recyclability are essential for industrial application. The spent $Au_{61}Pd_{39}$/Ce-NR catalyst was recycled after each 6-hour run with intermediate washing several times with water and ethanol, centrifuging and drying. The results are shown in Figure 6. Remarkably, after four catalytic cycles, the catalytic performance of $Au_{61}Pd_{39}$/Ce-NR was virtually unchanged – both in terms of activity as measured by conversion and selectivity to gluconic

acid. Metal leaching is typically the primary reason for catalyst deactivation in glucose oxidation. Glucose and the highly oxygenated reaction products are strong chelating agents that often accelerate the leaching of active metal components during the reaction (i.e. lixiviation). The pH of the reaction medium was measured at the end of each run and was found to be highly acidic (ca. pH= 2.5). Elemental analysis of the spent $Au_{61}Pd_{39}$/Ce-NR catalyst showed no significant metal loss after 4 catalytic cycles (see Table S1). The ability of the Ce-NR supported catalyst to resist deactivation and metal leaching even in the highly acidic environment of the final reaction mixture is certainly remarkable, although it is possible that deactivation would become observable with more extended recycling. Furthermore, selectivity to gluconic acid after the 4th cycle was essentially unchanged at >97%. Given our previous speculation discussed above that oxidation of gluconic to glucaric acid may involve a homogeneous catalytic component associated with leached Au clusters, the low selectivity to GLA even after four cycles is further evidence of the remarkable stability of the $Au_{61}Pd_{39}$/Ce-NR catalyst.

The leaching behavior of the $Au_{61}Pd_{39}$/Ce-NR catalyst is in sharp contrast to the behavior of $Au_{15}Pd_{85}$/Ti-NT where considerable leaching of both Au and Pd was observed over four cycles at the same reaction conditions leading to deactivation (see Figure 6 for comparison). Again, this underlines the greater stability of the ceria nanorod supported catalysts, which we attribute to the stronger metal-support interaction and the smaller NP size as discussed above.

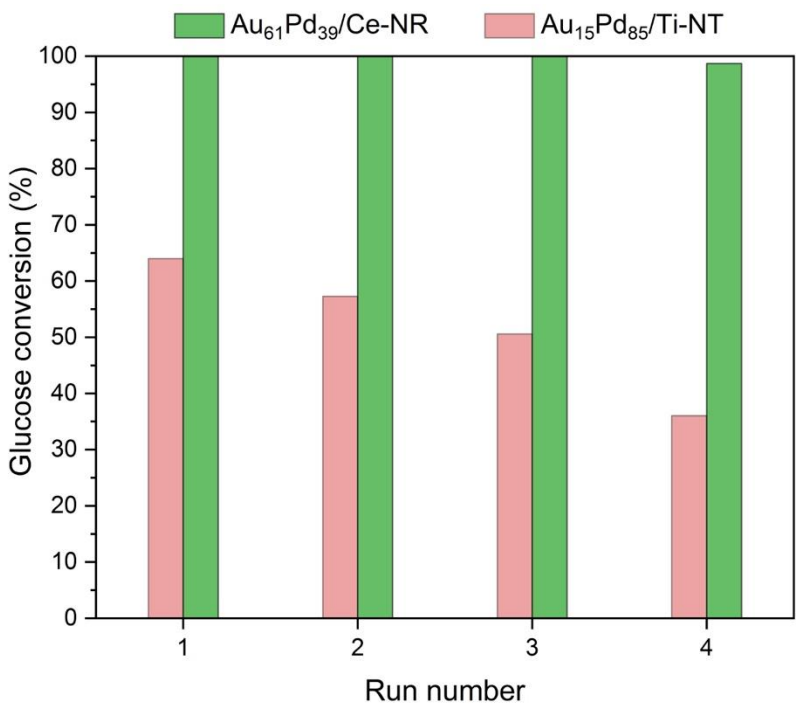

Figure 6 Glucose conversion for $Au_{61}Pd_{39}$/Ce-NR and $Au_{15}Pd_{85}$/Ti-NT over 4 runs. Reaction conditions: T= 80°C, pO_2 =6 bar, stirring rate=1000 rpm, glucose= 0.25M, $pH_{initial}$ = 9.5, glucose/metal = 100, time=6h. Recycling data for $Au_{15}Pd_{85}$/Ti-NT reproduced from ref. [22].

4. Conclusion

This work has demonstrated that ceria nanorod is an excellent support material for colloidal Au-Pd NPs. The catalytic activity of Au_xPd_y/Ce-NR was found to be strongly dependent on the bimetallic composition for the selective oxidation of glucose: Au-rich bimetallic catalysts were more active in glucose oxidation than Pd-rich catalysts, the most active being $Au_{61}Pd_{39}$/Ce-NR. Au_xPd_y/Ce-NR catalysts were highly selective for GLO in sharp contrast to previously reported Au_xPd_y/Ti-NT which are increasingly selective to GLA with increasing Au content [24]. Au-Pd supported on Ce-NR also exhibited superior activity in comparison to Au-Pd supported on Ti-NT or TiO_2. It is likely that the basicity of ceria and its ability to activate oxygen contribute to the enhanced activity of $Au_{61}Pd_{39}$/Ce-NR catalyst in comparison to Ti-NT or TiO_2-supported catalysts.

The most active glucose oxidation catalyst (i.e. $Au_{61}Pd_{39}$/Ce-NR) gave the same catalytic performance with no apparent deactivation or loss of Au or Pd on recycling 4 times. The outstanding activity, selectivity, and resistance to deactivation exhibited by $Au_{61}Pd_{39}$/Ce-NR in glucose oxidation is remarkable, and can be ascribed to interaction of the Au-Pd NPs with the surface of the Ce-NR. Defects on the Ce-NR surface are likely to serve as anchoring sites for Au-Pd NPs, leading to small NPs, and prevent leaching of Au or Pd into solution during glucose oxidation.

Acknowledgement

Motaz Khawaji gratefully acknowledges the financial support of Saudi Aramco. This work was funded in part by Saudi Aramco and EPSRC(UK) grant EP/K014749/1. We are grateful to Professor Graham Hutchings and Dr. Robert Armstrong from Cardiff Catalysis Institute for providing us with a sample of glucaric acid.

References

[1] J.N. Chheda, G.W. Huber, J.A. Dumesic, Liquid-Phase Catalytic Processing of Biomass-Derived Oxygenated Hydrocarbons to Fuels and Chemicals, Angewandte Chemie International Edition, 46 (2007) 7164-7183.

[2] A.M. Cañete-Rodríguez, I.M. Santos-Dueñas, J.E. Jiménez-Hornero, A. Ehrenreich, W. Liebl, I. García-García, Gluconic acid: Properties, production methods and applications—An excellent opportunity for agro-industrial by-products and waste bio-valorization, Process Biochemistry, 51 (2016) 1891-1903.

[3] Y. Önal, S. Schimpf, P. Claus, Structure sensitivity and kinetics of D-glucose oxidation to D-gluconic acid over carbon-supported gold catalysts, Journal of Catalysis, 223 (2004) 122-133.

[4] N. Thielecke, M. Aytemir, U. Prüsse, Selective oxidation of carbohydrates with gold catalysts: Continuous-flow reactor system for glucose oxidation, Catalysis Today, 121 (2007) 115-120.

[5] T. Werpy, G. Petersen, A. Aden, J. Bozell, J. Holladay, J. White, A. Manheim, D. Eliot, L. Lasure, S. Jones, Top Value Added Chemicals From Biomass. Volume 1 - Results of Screening for Potential Candidates From Sugars and Synthesis Gas, 2004.

[6] F.H. Isikgor, C.R. Becer, Lignocellulosic biomass: a sustainable platform for the production of bio-based chemicals and polymers, Polymer Chemistry, 6 (2015) 4497-4559.
[7] D.E. Kiely, L. Chen, T.H. Lin, Hydroxylated nylons based on unprotected esterified D-glucaric acid by simple condensation reactions, Journal of the American Chemical Society, 116 (1994) 571-578.
[8] C.L. Mehltretter, Process of making D-saccharic acid, US Patents, 1948.
[9] C.L. Mehltretter, C.E. Rist, Sugar Oxidation, Saccharic and Oxalic Acids by the Nitric Acid Oxidation of Dextrose, Journal of Agricultural and Food Chemistry, 1 (1953) 779-783.
[10] V. Thaore, D. Chadwick, N. Shah, Sustainable production of chemical intermediates for nylon manufacture: A techno-economic analysis for renewable production of caprolactone, Chemical Engineering Research and Design, 135 (2018) 140-152.
[11] V.B. Thaore, R.D. Armstrong, G.J. Hutchings, D.W. Knight, D. Chadwick, N. Shah, Sustainable production of glucaric acid from corn stover via glucose oxidation: an assessment of homogeneous and heterogeneous catalytic oxidation production routes, Chemical Engineering Research and Design (2019).
[12] J.M.H. Dirkx, H.S. van der Baan, The oxidation of gluconic acid with platinum on carbon as catalyst, Journal of Catalysis, 67 (1981) 14-20.
[13] M. Comotti, C.D. Pina, M. Rossi, Mono- and bimetallic catalysts for glucose oxidation, Journal of Molecular Catalysis A: Chemical, 251 (2006) 89-92.
[14] A. Abbadi, H. van Bekkum, Effect of pH in the Pt-catalyzed oxidation of d-glucose to d-gluconic acid, Journal of Molecular Catalysis A: Chemical, 97 (1995) 111-118.
[15] S. Biella, L. Prati, M. Rossi, Selective Oxidation of D-Glucose on Gold Catalyst, Journal of Catalysis, 206 (2002) 242-247.
[16] A. Mirescu, U. Prüße, A new environmental friendly method for the preparation of sugar acids via catalytic oxidation on gold catalysts, Applied Catalysis B: Environmental, 70 (2007) 644-652.
[17] H. Zhang, N. Toshima, Glucose oxidation using Au-containing bimetallic and trimetallic nanoparticles, Catalysis Science & Technology, 3 (2013) 268-278.
[18] C. Megías-Sayago, S. Ivanova, C. López-Cartes, M.A. Centeno, J.A. Odriozola, Gold catalysts screening in base-free aerobic oxidation of glucose to gluconic acid, Catalysis Today, 279 (2017) 148-154.
[19] R. Wojcieszak, I.M. Cuccovia, M.A. Silva, L.M. Rossi, Selective oxidation of glucose to glucuronic acid by cesium-promoted gold nanoparticle catalyst, Journal of Molecular Catalysis A: Chemical, 422 (2016) 35-42.
[20] Z. Zhang, P. Gibson, S.B. Clark, G. Tian, P.L. Zanonato, L. Rao, Lactonization and Protonation of Gluconic Acid: A Thermodynamic and Kinetic Study by Potentiometry, NMR and ESI-MS, Journal of Solution Chemistry, 36 (2007) 1187-1200.
[21] R.D. Armstrong, B.M. Kariuki, D.W. Knight, G.J. Hutchings, How to Synthesise High Purity, Crystalline d-Glucaric Acid Selectively, European Journal of Organic Chemistry, 2017 (2017) 6811-6814.
[22] M. Khawaji, Y. Zhang, M. Loh, I. Graça, E. Ware, D. Chadwick, Composition dependent selectivity of bimetallic Au-Pd NPs immobilised on titanate nanotubes in catalytic oxidation of glucose, Applied Catalysis B: Environmental, 256 (2019) 117799.
[23] D.V. Bavykin, F.C. Walsh, Titanate and Titania Nanotubes : Synthesis, Properties and Applications, 2009.
[24] M. Khawaji, D. Chadwick, Au-Pd Bimetallic Nanoparticles Immobilised on Titanate Nanotubes: A Highly Active Catalyst for Selective Oxidation, ChemCatChem, 9 (2017) 4353-4363.
[25] L. Qian, Z. Wang, E.V. Beletskiy, J. Liu, H.J. dos Santos, T. Li, M.d.C. Rangel, M.C. Kung, H.H. Kung, Stable and solubilized active Au atom clusters for selective epoxidation of cis-cyclooctene with molecular oxygen, Nature Communications, 8 (2017) 14881.
[26] M. Haruta, Size- and support-dependency in the catalysis of gold, Catalysis Today, 36 (1997) 153-166.

[27] S. Demirel, P. Kern, M. Lucas, P. Claus, Oxidation of mono- and polyalcohols with gold: Comparison of carbon and ceria supported catalysts, Catalysis Today, 122 (2007) 292-300.
[28] R. Si, M. Flytzani-Stephanopoulos, Shape and Crystal-Plane Effects of Nanoscale Ceria on the Activity of Au-CeO2 Catalysts for the Water–Gas Shift Reaction, Angewandte Chemie International Edition, 47 (2008) 2884-2887.
[29] H. Zhang, Y. Xie, Z. Sun, R. Tao, C. Huang, Y. Zhao, Z. Liu, In-Situ Loading Ultrafine AuPd Particles on Ceria: Highly Active Catalyst for Solvent-Free Selective Oxidation of Benzyl Alcohol, Langmuir, 27 (2011) 1152-1157.
[30] Z. Hu, X. Liu, D. Meng, Y. Guo, Y. Guo, G. Lu, Effect of Ceria Crystal Plane on the Physicochemical and Catalytic Properties of Pd/Ceria for CO and Propane Oxidation, ACS Catalysis, 6 (2016) 2265-2279.
[31] M. Khawaji, D. Chadwick, Au–Pd NPs immobilised on nanostructured ceria and titania: impact of support morphology on the catalytic activity for selective oxidation, Catalysis Science & Technology, 8 (2018) 2529-2539.
[32] X. Liu, K. Zhou, L. Wang, B. Wang, Y. Li, Oxygen Vacancy Clusters Promoting Reducibility and Activity of Ceria Nanorods, Journal of the American Chemical Society, 131 (2009) 3140-3141.
[33] J.M. López, A.L. Gilbank, T. García, B. Solsona, S. Agouram, L. Torrente-Murciano, The prevalence of surface oxygen vacancies over the mobility of bulk oxygen in nanostructured ceria for the total toluene oxidation, Applied Catalysis B: Environmental, 174 (2015) 403-412.
[34] M. Khawaji, D. Chadwick, Front cover, Catalysis Science & Technology, 8 (2018) 2505-2506.
[35] M. Khawaji, D. Chadwick, Selective oxidation using Au-Pd catalysts: role of the support in the stabilization of colloidal Au-Pd NPs, Catalysis Today, (2019).
[36] H.-X. Mai, L.-D. Sun, Y.-W. Zhang, R. Si, W. Feng, H.-P. Zhang, H.-C. Liu, C.-H. Yan, Shape-Selective Synthesis and Oxygen Storage Behavior of Ceria Nanopolyhedra, Nanorods, and Nanocubes, The Journal of Physical Chemistry B, 109 (2005) 24380-24385.
[37] L. Torrente-Murciano, A. Gilbank, B. Puertolas, T. Garcia, B. Solsona, D. Chadwick, Shape-dependency activity of nanostructured CeO2 in the total oxidation of polycyclic aromatic hydrocarbons, Applied Catalysis B: Environmental, 132 (2013) 116-122.
[38] A. Galtayries, R. Sporken, J. Riga, G. Blanchard, R. Caudano, XPS comparative study of ceria/zirconia mixed oxides: powders and thin film characterisation, Journal of Electron Spectroscopy and Related Phenomena, 88-91 (1998) 951-956.
[39] A.I.Y. Tok, S.W. Du, F.Y.C. Boey, W.K. Chong, Hydrothermal synthesis and characterization of rare earth doped ceria nanoparticles, Materials Science and Engineering: A, 466 (2007) 223-229.
[40] B. Pawelec, A.M. Venezia, V. La Parola, E. Cano-Serrano, J.M. Campos-Martin, J.L.G. Fierro, AuPd alloy formation in Au-Pd/Al2O3 catalysts and its role on aromatics hydrogenation, Applied Surface Science, 242 (2005) 380-391.
[41] K. Mori, T. Hara, T. Mizugaki, K. Ebitani, K. Kaneda, Hydroxyapatite-Supported Palladium Nanoclusters: A Highly Active Heterogeneous Catalyst for Selective Oxidation of Alcohols by Use of Molecular Oxygen, Journal of the American Chemical Society, 126 (2004) 10657-10666.
[42] C.W. Yi, K. Luo, T. Wei, D.W. Goodman, The Composition and Structure of Pd−Au Surfaces, The Journal of Physical Chemistry B, 109 (2005) 18535-18540.
[43] M. Besson, F. Lahmer, P. Gallezot, P. Fuertes, G. Fleche, Catalytic Oxidation of Glucose on Bismuth-Promoted Palladium Catalysts, Journal of Catalysis, 152 (1995) 116-121.
[44] H. Zhang, T. Watanabe, M. Okumura, M. Haruta, N. Toshima, Catalytically highly active top gold atom on palladium nanocluster, Nature Materials, 11 (2011) 49.
[45] Z. Wu, A.K.P. Mann, M. Li, S.H. Overbury, Spectroscopic Investigation of Surface-Dependent Acid–Base Property of Ceria Nanoshapes, The Journal of Physical Chemistry C, 119 (2015) 7340-7350.
[46] J.C. González, J.C. Hernández, M. López-Haro, E. del Río, J.J. Delgado, A.B. Hungría, S. Trasobares, S. Bernal, P.A. Midgley, J.J. Calvino, 3 D Characterization of Gold Nanoparticles Supported on Heavy Metal Oxide Catalysts by HAADF-STEM Electron Tomography, Angewandte Chemie, 121 (2009) 5417-5419.

[47] J. Lee, B. Saha, D.G. Vlachos, Pt catalysts for efficient aerobic oxidation of glucose to glucaric acid in water, Green Chemistry, 18 (2016) 3815-3822.
[48] X. Jin, M. Zhao, J. Shen, W. Yan, L. He, P.S. Thapa, S. Ren, B. Subramaniam, R.V. Chaudhari, Exceptional performance of bimetallic Pt1Cu3/TiO2 nanocatalysts for oxidation of gluconic acid and glucose with O2 to glucaric acid, Journal of Catalysis, 330 (2015) 323-329.